SPECTROSCOPIC MEASUREMENTS OF TROPOSPHERIC COMPOSITION FROM SATELLITE MEASUREMENTS IN THE ULTRAVIOLET AND VISIBLE: STEPS TOWARD CONTINUOUS POLLUTION MONITORING FROM SPACE

SHORT TITLE: UV/VISIBLE ATMOSPHERIC MEASUREMENTS FROM SPACE

KELLY CHANCE
Harvard-Smithsonian Center for Astrophysics, Atomic and Molecular Physics Division, 60 Garden Street, Cambridge, MA, 02138, USA

Abstract. This chapter reviews the current capabilities for ultraviolet and visible spectroscopic measurements of the Earth's troposphere, and discusses what remains to be achieved in the short term to enable global, continuous measurements of atmospheric pollution from space to be undertaken. Challenges in instrumentation, spectroscopy, radiative transfer modeling, and retrievals are discussed. Current and planned satellite instruments with the capability to make tropospheric measurements in the ultraviolet and visible, with their measurement properties, spectral coverage, and target molecules, are presented. Measurement examples are taken from recent work done at the Harvard-Smithsonian Center for Astrophysics, together with our colleagues at a number of institutions. The examples include global tropospheric ozone (O_3) measurements from the nadir geometry; global tropospheric nitrogen dioxide (NO_2); bromine oxide (BrO) in the polar spring, and from salt lakes and volcanoes; global tropospheric formaldehyde (HCHO); and preliminary measurements of glyoxal (CHOCHO). Except for a few remaining developments, the field is shown to be sufficiently mature that global measurements of atmospheric pollution from space may be undertaken.

Keywords: ultraviolet spectroscopy; visible spectroscopy; atmospheric remote sensing; tropospheric composition; radiative transfer modeling; chemistry and transport modeling

Journal Information

1. Introduction

Since the Scanning Imaging Absorption Spectrometer for Atmospheric Chartography (SCIAMACHY) instrument was proposed[1,2] the capability to measure tropospheric pollutants other than ozone (*cf*. Refs. 3,4) and volcanic sulfur dioxide (SO_2; *cf*. ref. 5) from space using ultraviolet and visible spectroscopy has gradually become established.

It is now possible to make tropospheric measurements of a number of chemical constituents, and to study their sources, sinks, transport, and transformation. This provides critical information on tropospheric oxidation chemistry and pollution of the lower atmosphere, and contributes to process studies, including intercontinental transport of pollution. In addition to O_3 and volcanic SO_2, there are limited measurements of anthropogenic SO_2,[6] as well as the examples cited in the abstract, which are discussed in more detail below. Aerosol and cloud measurements in the ultraviolet and visible are not included here although they are, of course, also of primary importance. In particular, cloud measurements may now be made using spectroscopic methods.[7]

This chapter provides an overview of current results and capabilities which show how ultraviolet and visible spectroscopy is used to elucidate important properties about the Earth's troposphere. This is now a sizable field of research, with some dozen Earth satellites now performing measurements or being planned or prepared for launch. This review uses examples from research done at the Harvard-Smithsonian Center for Astrophysics (CfA), http://cfa-www.harvard.edu/atmosphere/, along with our collaborators. It is not fully inclusive of techniques, groups, and results, due to space limitations. It is intended to summarize many of the technical issues involved in data analysis, show by example the power of this type of measurement, and provide a convenient starting place for further inquiries. There are a number of other active groups performing similar and related work whose websites should be consulted for a broader view.[8]

An overview of the UV/visible atmosphere and the basic measurement techniques is presented, followed by a discussion of issues in algorithm physics, a survey of current and planned instruments, and illustrative examples of the application of UV/visible measurements to tropospheric process studies. The paper will conclude with a brief synopsis of the current state of measurements with respect to requirements for global pollution monitoring from satellites in geostationary orbits.

A distinction is made here between a spectrometer, which makes spectroscopic measurements over a substantial wavelength range at moderate to high spectral resolution, normally of multiple species when being used as an atmospheric instrument, and an instrument measuring at several wavelength

bands to measure (normally) one species. Instruments at both extremes have contributed historically and continue to do so, although there is a marked tendency in the UV/visible to now employ spectrometers with array-type detectors to cover large portions of the spectrum at 0.2-1.0 nm spectral resolution. These measurements are emphasized here.

2. The UV/Visible Atmosphere

The solar spectrum can be roughly approximated as a blackbody at 5900 K. The reality, for detailed spectroscopic measurements, is much more complicated. Figure 1 (top) shows a low resolution extraterrestrial solar spectrum (the Fraunhofer spectrum) over much of the UV/visible region;[9-11] Figure 1 (bottom) shows a detailed section of the solar spectrum in a region where NO_2 is commonly measured from space.[9] The source spectrum is seen to be quite complex. To the extent that measurements correspond to simple Bouguet (or Lambert-Beer) absorption this would not present a particular difficulty. In practice, because of the Ring effect (discussed below in **Algorithm Physics**), a detailed knowledge of the solar spectrum is required, particularly for some of the molecules with small absorption: These molecules (including NO_2, BrO, HCHO, CHOCHO, SO_2, and, in parts of the spectrum, O_3) are the most important tropospheric species to be measured from space in this spectral region.

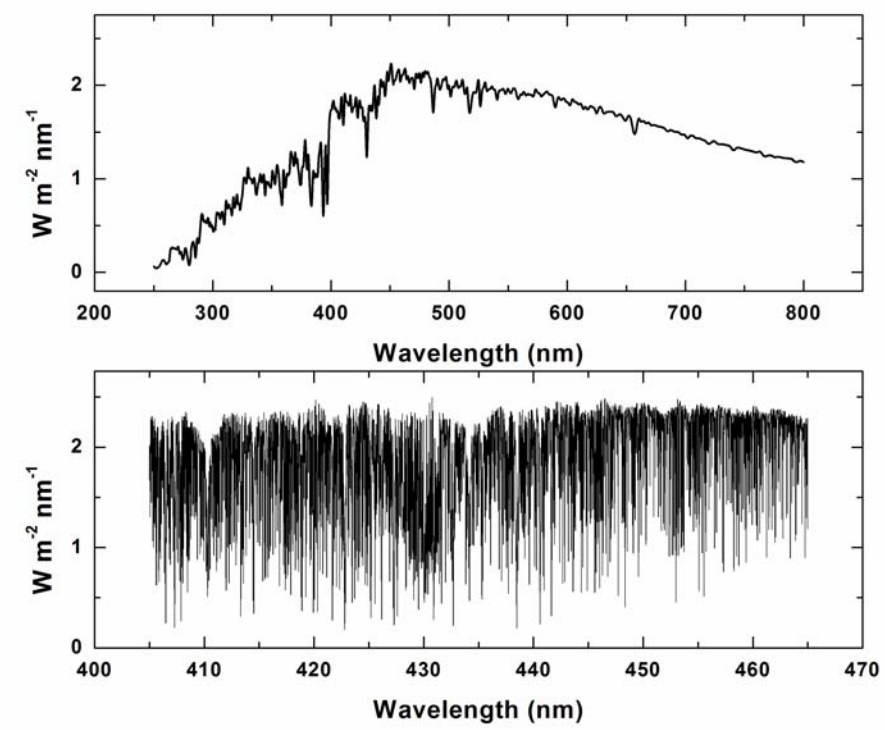

Figure 1. The low resolution extraterrestrial solar spectrum over much of the UV/visible region (top); a detailed section of the solar spectrum in a region where NO_2 is commonly measured from space (bottom).

Figure 2 shows an overview of the absorptions due to molecules that are now commonly measured from space in the nadir geometry. Absorptions are for typical measurement geometry and atmospheric concentrations and, for tropospheric gases, under conditions of moderate enhancement, except that SO_2 is increased to an amount typical for a volcanic source and ClO and OClO (stratospheric species) are increased to amounts typically seen in the Antarctic polar vortex. The effects of clouds and of Rayleigh scattering can be gauged from Figure 3, which shows back scattered albedo spectra ($\equiv \pi R/\mu_0 I_0$, where R is the radiance, μ_0 the cosine of the solar zenith angle, and I_0 the irradiance) from Global Ozone Monitoring Experiment (GOME) measurements[12] for two extreme examples. The highest albedo scene, corresponding to full coverage by high clouds, is white and quite bright, due to the cloud reflectance; the lowest albedo case is a cloud-free scene over the ocean illustrating the low reflectance by water (less than 2% at the infrared end) and the increasing contribution from Rayleigh scattering at shorter wavelengths, as the radiation penetrates to lower

altitudes for this cloud-free scene. The inverted Fraunhofer structure in these spectra, most visible below 400 nm, is due to the incomplete cancellation of the structure cause by the Ring effect, discussed below.

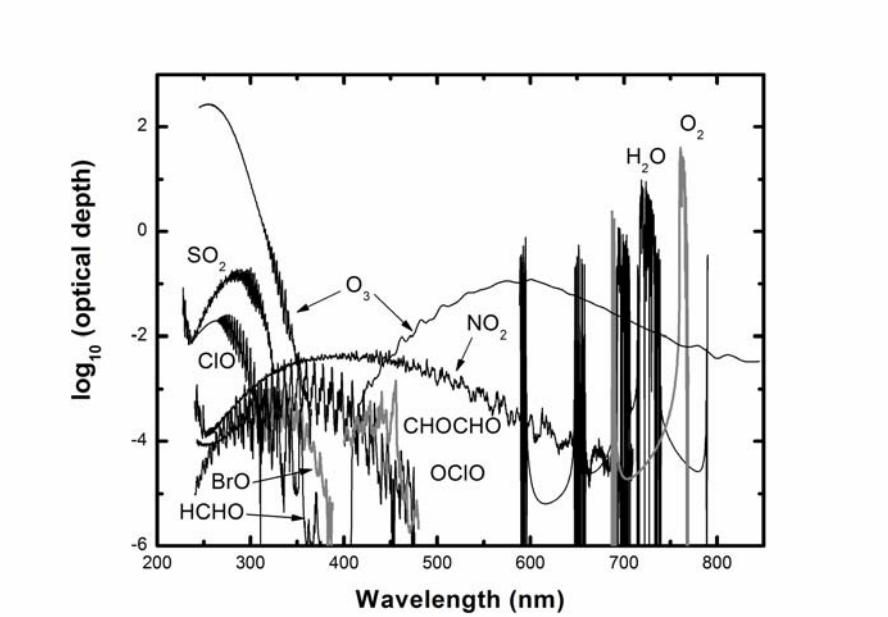

Figure 2. Typical absorptions due to molecules that are now commonly measured from space in the nadir geometry.

3. Measurement Techniques

UV/visible measurements of the atmosphere are made in one of three basic measurement geometries: 1. Nadir - the back scattered light is measured in a geometry where the line of sight intersects the Earth's surface. The light source is solar radiation back scattered from a combination of surface reflectance and cloud, aerosol and Rayleigh scattering. 2. Occultation - The light source is direct illumination by the Sun (or, less frequently, the Moon or stars). 3. Limb scattering - The light source is Rayleigh scattering of solar light in the limb geometry. Information from occultation and limb scattering measurements is generally limited to the stratosphere and upper troposphere. Most of the information on tropospheric composition, particularly for lower tropospheric pollution studies, comes from nadir measurements although, for O_3 and NO_2,

the use of limb-nadir subtraction has been investigated for use in improving tropospheric retrievals.[13]

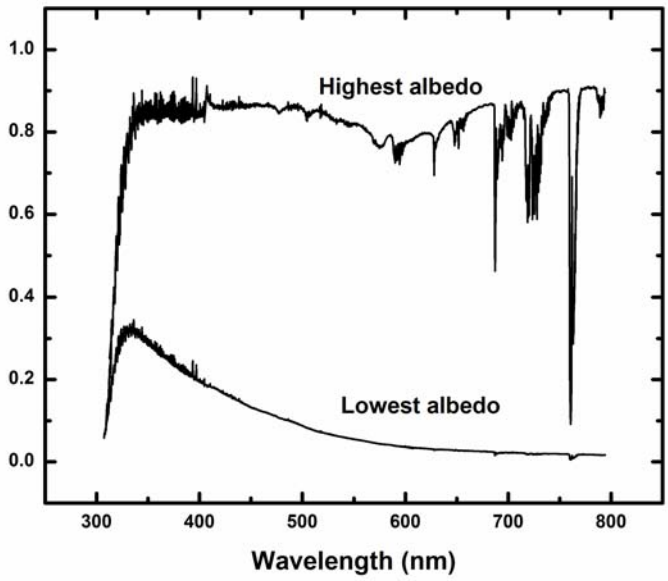

Figure 3. Back scattered albedo spectra from GOME measurements for two extreme examples. The highest albedo scene, corresponding to full coverage by high clouds, is white and quite bright, due to the cloud reflectance; the lowest albedo case is a cloud-free scene over the ocean.

Analysis of nadir measurements is most commonly made using either fitting to determine a total slant column (SC) abundance, followed by adjustment to determine the vertical column (VC) abundance, or by directly fitting to details in the spectrum to determine a vertical column amount or profile.

For slant column measurements, spectra may be fitted by a variety of methods, ranging from directly fitting to the radiance[14] to fitting of a low-pass filtered version of $ln(R/I_0)$ (*i.e.*, DOAS[15]). Vertical column abundances are then determined by division of the SC by an Air Mass Factor (AMF), which is simply the ratio of the slant to vertical column, determined from knowledge of the vertical distribution, either from climatology or from assimilation of data into chemistry and transport modeling,[16,17] and radiative transfer calculation to take into account Rayleigh and other scattering as well as the spherical

atmospheric geometry (*cf*. Refs. 15,16). There may be further correction to account for the (sometimes strong) variation of the AMF over the spectral fitting window. It is also possible to obtain vertical column abundances directly, by including the radiative transfer modeling inside of the fitting procedure.[18]

It was discovered by Singer and Wentworth[19] that Rayleigh scattering, which often complicates retrieval due to its strong ($\approx 1/\lambda^4$) dependence on wavelength, could also serve as a source of information. In the strong Hartley band of ozone at wavelengths <300 nm, back scattered radiation from nadir measurements has not penetrated to the Earth's surface. The source of illumination is Rayleigh scattering. Light of different wavelengths penetrates to different atmospheric depths, depending on the measurement geometry, the strength of the scattering, and the wavelength dependence of the O_3 absorption: The spectrum can be inverted to give a stratospheric ozone profile. This is the basis for BUV/SBUV measurements of ozone profiles.[20] The greater wavelength coverage and higher spectral resolution of more modern spectrometers can improve the situation further. During the sensitivity analyses performed when the SCIAMACHY instrument was being proposed, it was discovered that adding detailed measurements of the strongly temperature-dependent Huggins bands of ozone to the BUV information makes it possible to determine the full atmospheric profile, which includes the tropospheric ozone abundance, directly.[2,21] This has been the basis of retrievals now successfully made using spectra from the GOME and SCIAMACHY satellite instruments, discussed below in **Examples**.

4. Algorithm Physics

A number of the technical challenges have had to be addressed in order to successfully analyze UV/visible atmospheric spectra from satellites to the fine level of agreement (as low as several times 10^{-4} of measured radiances in favorable cases[14]) needed for use in atmospheric process studies, and to permit retrievals of ozone profiles and tropospheric ozone to the maximum altitude resolution that the physics in the spectroscopy and radiative transfer permits.

4.1. SOLAR REFERENCE SPECTRA

An extraterrestrial high resolution solar spectrum would be invaluable for the spaceborne measurements. Such a spectrum is needed for wavelength calibration,[22] Ring effect determination,[23-25] determination of the instrument transfer function from flight data, and correction for spectral undersampling.[14,26] Since an appropriate extraterrestrial spectrum does not exist (the extensive SOLSTICE/SUSIM measurements of Ref. 10 are very good in absolute

intensity calibration, but have much too low spectral resolution to be used for these purposes), ground-based FTS spectra, in particular a solar spectrum from Kurucz *et al*. at the National Solar Observatory (NSO)[9] has been used extensively, supplemented at wavelengths <305 nm by balloon-based spectra from Hall and Anderson.[27]

4.2. RAYLEIGH SCATTERING AND THE RING EFFECT

Rayleigh scattering is a major contributor, sometimes the predominant contributor, to back scattered light measured in the nadir, depending on wavelength and detailed measurement geometry. For limb measurements, it is the source of the measured light, except for aerosol contributions at lower altitudes. Highly accurate formulations of the wavelength dependences of the cross sections and scattering phase function for Rayleigh scattering by air are available.[24,28,29]

The Ring effect was first noted by Grainger and Ring[30] as a broadening and reduction in depth of solar Fraunhofer lines when viewed from the ground in scattered sunlight. It has now been firmly demonstrated to be the effect of the fraction of Rayleigh scattering by air that is inelastic, *i.e.*, Raman scattering. The Raman scattering is predominantly rotational Raman; it constitutes 4% of the Rayleigh scattering in the UV/visible. Ring effect corrections may now be performed using the molecular physics of the Raman scattering coupled with a suitable solar reference spectrum,[24] in some cases coupled with radiative transfer calculations,[23,25] to the level that negligible uncertainties remain in the spectral fitting from this source of spectral structure.

Vibrational Raman scattering in ocean water can be readily sensed in the UV/visible (it must be corrected for in the spectral analysis for some gases) and it has been suggested that it may be used to "estimate chlorophyll and dissolved organic matter contents" of ocean water.[31]

4.3. WAVELENGTH ISSUES

Ground-based wavelength calibration is insufficient for detailed spectrum fitting of satellite data for several reasons. First, calibration can shift substantially due to launch stresses; second, calibration in flight can vary by substantial amounts, compared to the spectral fitting needs, due to thermal and other in-flight perturbations and instrumental effects (*e.g.*, partial filling of the field-of-view); third, solar irradiances and radiances are often obtained (especially for nadir observations) at substantially different Doppler shifts (up to 0.01 nm at 400 nm). For these reasons, methods were developed first for GOME in-flight spectral calibration, using nonlinear least-squares (NLLS)

minimization or spectral cross correlation, where the comparison spectrum in both cases is derived from the NSO spectrum described above.[22] The NLLS method is now used extensively in scientific analyses, and has been implemented in operational algorithms for GOME, SCIAMACHY, the Ozone Monitoring Instrument (OMI), and the Ozone Mapping and Profiler Suite (OMPS).

4.4. REFERENCE SPECTRA

Reference spectra for UV/visible measurements are now included in the HITRAN database,[32,33] and regularly updated. Reference spectra are published sometimes with vacuum wavelengths and sometimes with air wavelengths (often with insufficient detail of laboratory conditions to allow accurate conversion to vacuum). It is highly recommended that vacuum wavelengths be the standard, and that accurate conversion be made when necessary. Highly accurate conversion formulae are available.[29] As UV/visible reference spectra are increasingly determined using Fourier transform spectrometers, this becomes less of an issue, since they measure frequencies, usually in wavenumbers (cm^{-1}), and these are intrinsically in vacuum.

4.5. INSTRUMENT FUNCTION AND SAMPLING ISSUES

Slit functions (instrument transfer functions, ITFs) in flight may differ from those determined in ground calibration. It is often useful to re-determine them in flight. The normal procedure is to combine this fitting with the wavelength calibration using NLLS, where the reference spectrum is a high-resolution solar spectrum.[14] Spectral undersampling occurs in array-based instruments (or indeed any spectrometer) when spectral measurements are not made at fine enough spacing to Nyquist sample the ITF,[34] and thus provide full knowledge of the spectrum up to the band limit (Nyquist sampling requires sampling to at least twice the highest spatial (*i.e.*, wavelength) frequency admitted by the resolution limit of the instrument). It can be a major source of fitting error in the current generation of satellite-borne spectrometers, particularly as solar irradiance spectra must be resampled in order to be compared to radiances in the spectral fitting process.[14] Where the trace gas absorptions are optically thin, it is possible to effectively correct for most of the undersampling error.[14,35] It is now possible to quantitatively determine the amount a spectrum will be undersampled (or, how close it is to being fully-sampled) for a given instrument configuration during the design phase.[26]

4.6. RADIATIVE TRANSFER MODELING AND CHEMISTRY AND TRANSPORT MODELING

Radiative transfer calculations, usually requiring multiple scattering treatment, and often needing spherical correction or inclusion of polarization, are fundamental to the analysis of UV/visible measurements in nadir and limb geometries. Radiative transfer models are now available for most UV/visible measurement situations.[36-43]

Primarily because of the interference by Rayleigh scattering with geometrical scattering paths in nadir measurements, particularly for tropospheric measurements, it is often necessary to couple radiative transfer calculations with chemistry and transport modeling in order to determine AMFs: The contribution of molecular absorption to backscattered radiance depends significantly on the absorber altitude. Generally, absorbers at lower altitudes contribute less to the observed signal (*cf*. Ref. 16). The GEOS-CHEM and MOZART 3-D tropospheric chemistry and transport models[44-46] are in common use for this purpose.

5. Current and planned instruments

A series of satellite instruments which measured in discrete (sometimes scannable) spectral bands formed the foundation for the present generation of satellite spectrometers which are capable of making extensive tropospheric measurements. The BUV/SBUV instruments, 1970-present (*cf*. Ref. 47) and the TOMS instruments, 1978-present (*cf*. Ref. 48) are predecessors of current spectroscopic UV/visible nadir instruments. Current and planned instruments are summarized in Table1.

TABLE 1. Current and planned UV/visible satellite spectrometers for tropospheric measurements

Instrument	*Nadir Wavelength Range (nm)*	*Tropospheric Gases*	*Launch year*
GOME/ERS-2; GOME-2 (×3)/MetOp	240-790	O_3, NO_2, BrO, SO_2, HCHO, CHOCHO, H_2O,	1995; 2006+
SCIAMACHY/Envisat	240-2340	O_3, NO_2, BrO, SO_2, HCHO, CHOCHO, H_2O (plus infrared gases)	2002
OMI/EOS-Aura	270-500	O_3, NO_2, BrO, SO_2, HCHO, CHOCHO	2004
OPUS/GCOM	306-420	O_3, NO_2, BrO, OClO, SO_2, HCHO	2007
OMPS/NPP-NPOESS	250-380	O_3, NO_2, BrO, OClO, SO_2,	2008+

(×4)	HCHO, H_2O

6. Application of UV/Visible Measurements to Tropospheric Process Studies

6.1. GLOBAL TROPOSPHERIC OZONE MEASUREMENTS FROM THE NADIR GEOMETRY

Initial sensitivity studies for GOME and SCIAMACHY indicated that tropospheric ozone could be measurable globally.[2,21] This was first demonstrated with GOME flight data by the Rutherford Appleton Laboratory,[49] and has since been implemented by several other groups, including our work at the CfA[50,51], the University of Bremen, the Space Research of the Netherlands, and the Royal Dutch Meteorological Institute.[8] Research at the CfA includes full profiles of ozone from nadir measurements by GOME and SCIAMACHY, as well as integrated tropospheric column ozone, and the capability to sample the ozone profiles at selected pressures or altitudes. The application of ozone profiling and tropospheric ozone algorithms to measurements from the OMI instrument is expected to begin in the near future. Figure 4 shows ozone profiles for a full orbit of GOME data on October 22, 1997 (an ozone hole orbit). The stratospheric ozone hole is clearly visible below ~70°S. Significant tropospheric ozone enhancements are visible over the Southern Indian Ocean and Indonesia, due in both cases to biomass burning.[50] Figure 5 shows monthly mean global tropospheric column ozone from the GOME instrument for October, 1997, where the columns are integrated to the NCEP tropopause height. The ozone distribution shows the well-known wave-1 pattern in the tropics, enhanced in the southern tropics particularly by biomass burning, and a strong band of ozone near 30°S, associated with the Hadley circulation. For a more detailed discussion see Ref. 51. (Figures 4 and 5 courtesy of X. Liu.)

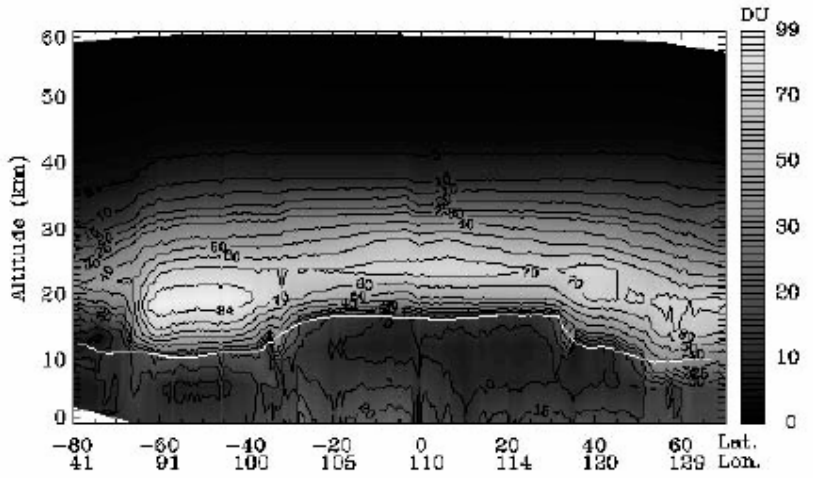

Figure 4. Ozone profiles for an orbit of GOME measurements on October 22, 1997 showing the Antarctic ozone hole and significant tropospheric enhancements over the Southern Indian Ocean and Indonesia.

6.2. GLOBAL TROPOSPHERIC NO_2

Nitrogen dioxide is the primary measurable proxy for NO_x, the reactive nitrogen pollutants.[8,17,52,53] Satellite measurements are used to track pollution and to improve global NO_x emission inventories,[54-56] and for other detailed process studies, such as the release of NO_x from soils,[57] and to investigate evidence of lightning NO_x and convective transport of pollutants.[58]

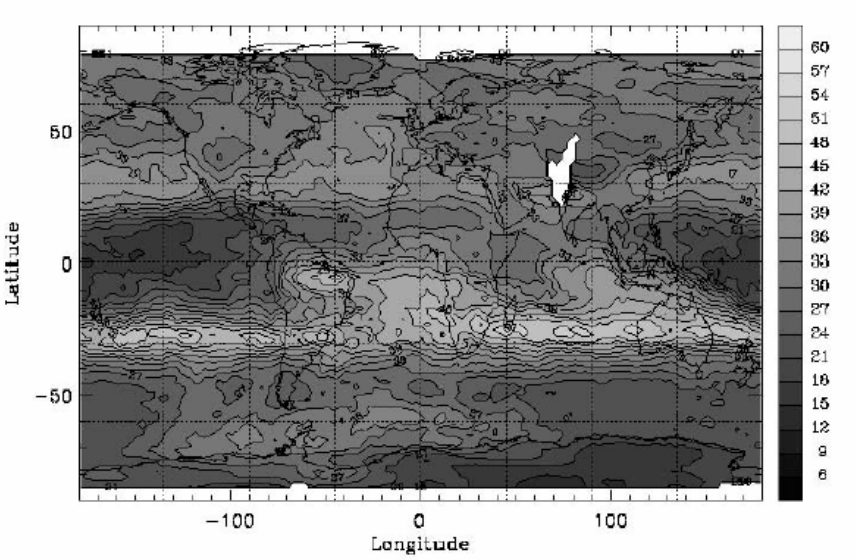

Figure 5. Monthly mean global tropospheric column ozone from the GOME instrument for October, 1997, where the columns are integrated to the NCEP tropopause height.

Figure 6 shows global and North American tropospheric NO_2 derived from SCIAMACHY measurements for May-October 2004, during the 2004 International Consortium for Atmospheric Research on Transport and Transformation (ICARTT) campaign. Intense sources reflect human activity: Urban areas to quite modest size are readily measurable. (Figure courtesy of R.V. Martin and C.E. Sioris.)

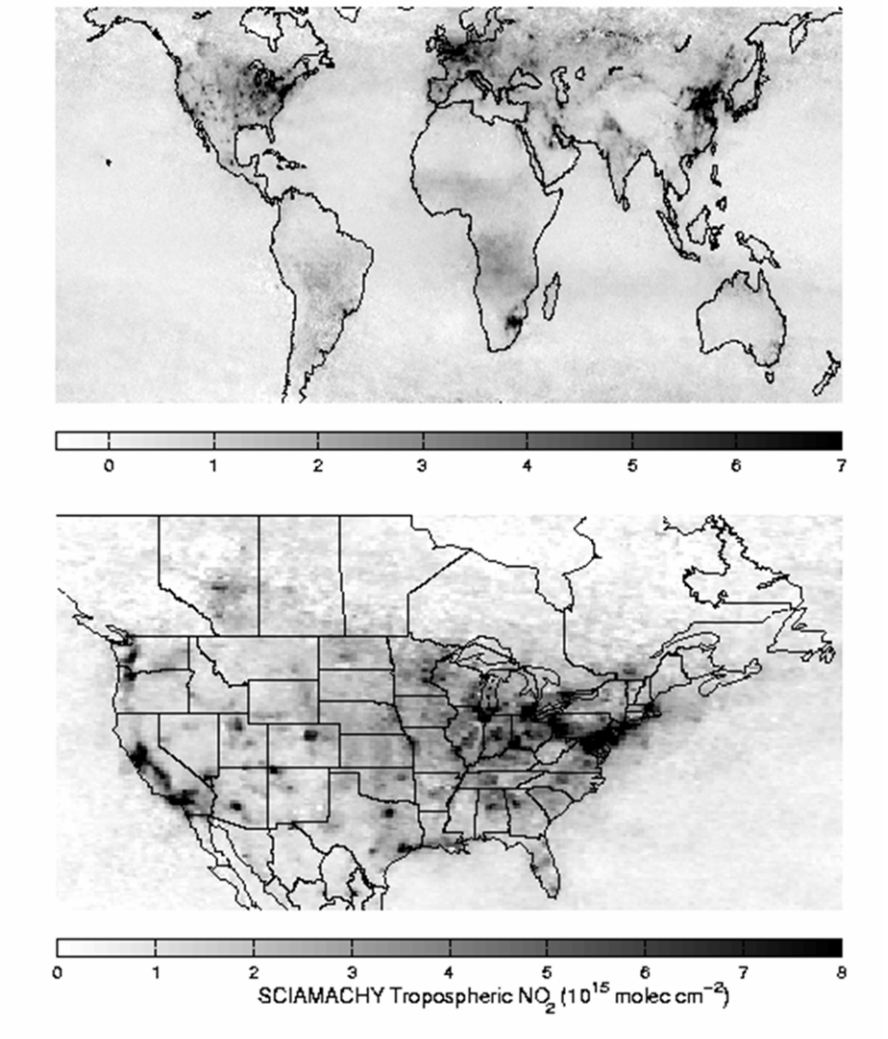

Figure 6. Global and North American tropospheric NO_2 from SCIAMACHY during the 2004 ICARTT campaign.

6.3. BRO IN THE POLAR SPRING, AND FROM SALT LAKES AND VOLCANOES

Initial sensitivity studies for GOME and SCIAMACHY indicated that stratospheric BrO could be measurable globally.[2] It was later discovered from ground-based measurements,[59] and then confirmed by GOME measurements,[8,14] that BrO is released copiously from the ice pack in polar spring, in both hemispheres, with implications for ozone depletion in the polar boundary layer (*cf*. Ref. 60). More recently, BrO has been measured using ground-based spectroscopy from halogen emission over the Dead Sea and the Great Salt Lake,[61,62] and from a volcanic plume.[63] Figure 7 shows BrO derived from OMI spectra over the shelf ice in Antarctica in the Southern Hemisphere spring (left) and for a partial orbit over Hudson Bay, Canada during the Northern Hemisphere Spring (right). Figure 8 shows BrO from OMI over the Dead Sea (left) and the Great Salt Lake (right). Figure 9 shows BrO from OMI from February 2005 during the eruption of the Ambrym Volcano, Vanuatu (16.25°S, 168.12°E). The striping in the images, most obvious in the Figure 7 (right) is an artifact due to incomplete calibration in the Level 1 (*i.e*., spectral) data products. It should be absent in future versions of the data products. (Figures 7-9 courtesy of T.P. Kurosu.)

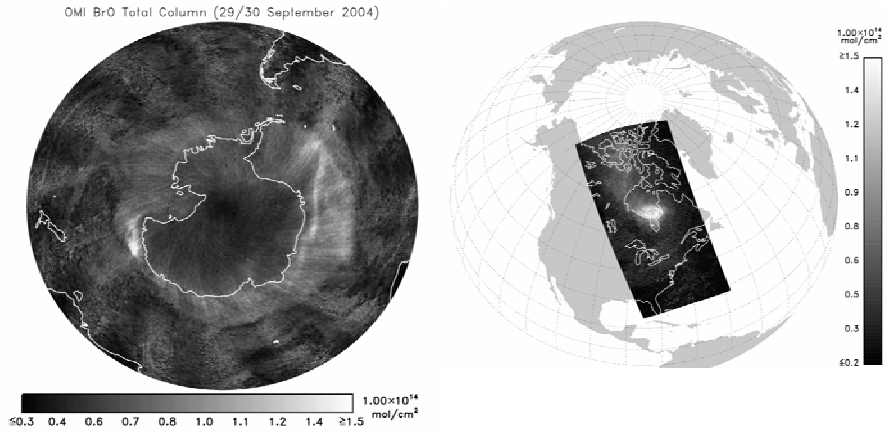

Figure 7. BrO from OMI over the shelf ice in Antarctica in the Southern Hemisphere spring (left) and for a partial orbit over Hudson Bay, Canada during the Northern Hemisphere Spring (right).

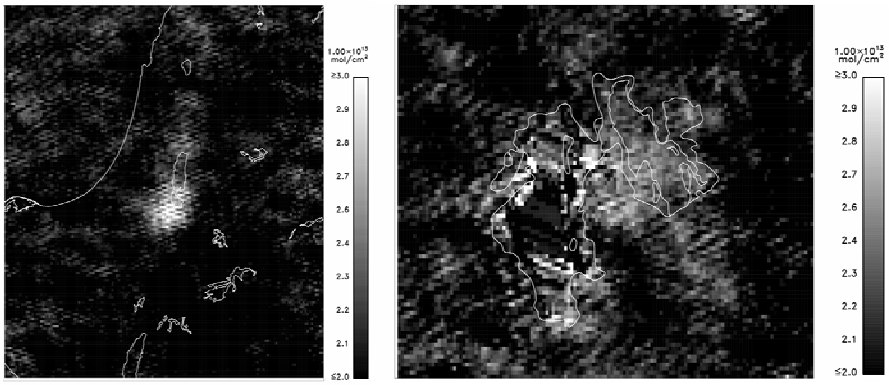

Figure 8. BrO from OMI over the Dead Sea (left) and the Great Salt Lake (right).

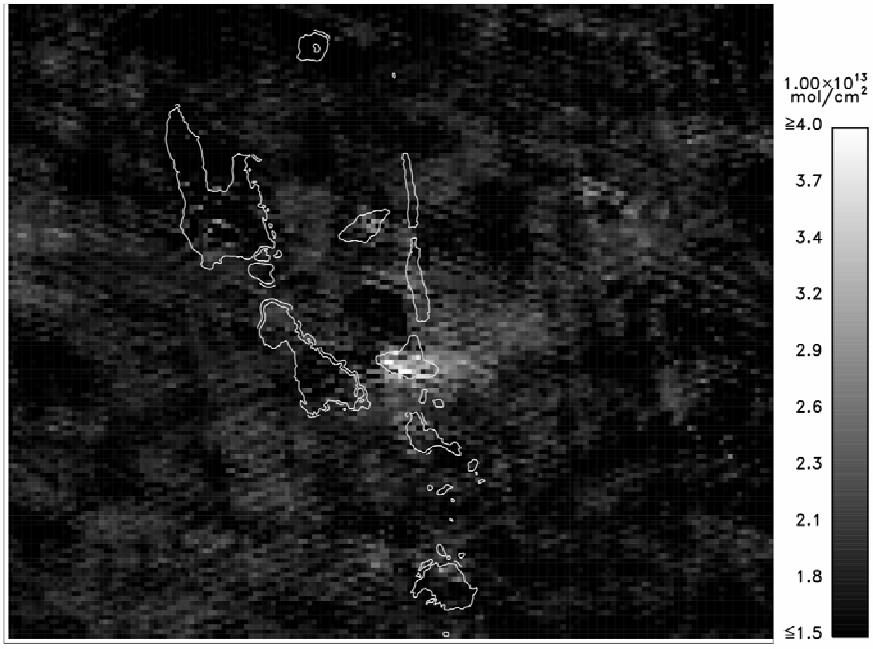

Figure 9. BrO from OMI from February 2005 during the eruption of the Ambrym Volcano, Vanuatu.

6.4. GLOBAL TROPOSPHERIC HCHO

Formaldehyde is currently the primary measurable proxy for volatile organic compounds, VOCs. Tropospheric HCHO measurements derived from GOME have been used to improve VOC emission inventories.[16,52,55,64-67] OMI measurements, which have much higher spatial resolution, show promise for substantially improving the knowledge of VOC emission sources. Figure 10 (left) shows tropospheric HCHO measurements from OMI for summertime (July 2005) over the U.S., where isoprene from trees is the major source, and (right) for Southeast Asia in October 2005, where sources include vegetation, biomass burning, and human activity (agriculture, fossil-fuel use). As with BrO, the Southeast Asia image still contains some residual striping. (Figure courtesy of T.P. Kurosu.)

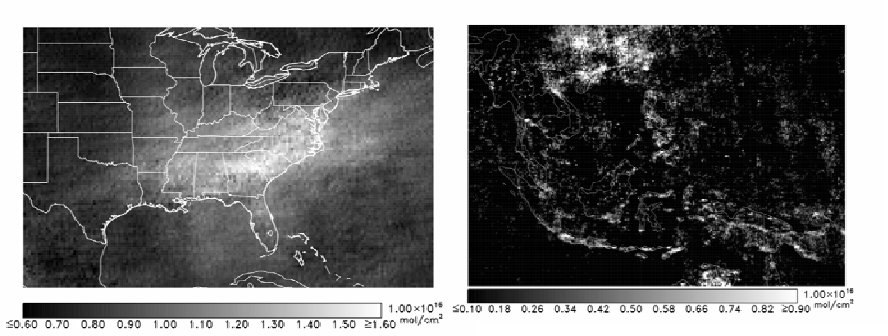

Figure 10. Tropospheric HCHO measurements from OMI for summertime (July 2005) over the U.S., where isoprene from trees is the major source (left), and for Southeast Asia in October 2005, where sources include vegetation, biomass burning, and human activity (right).

6.5. PRELIMINARY MEASUREMENTS OF CHOCHO

CHOCHO is another high-yield product of VOC oxidation, although it has significantly difference source chemistry and a significantly shorter atmospheric lifetime than HCHO. As such, it can provide a probe for VOC emissions with different characteristics than HCHO. CHOCHO has recently been measured in Mexico City using ground-based spectroscopy.[68] Research at the CfA has now shown that CHOCHO can be successfully measured from space, although measurements are preliminary as the algorithm is still undergoing optimization. Figure 11 shows elevated CHOCHO over the Guangzhou, China area in July, 2005. As with BrO and HCHO, some residual striping is evident. (Figure courtesy of T. Kurosu.)

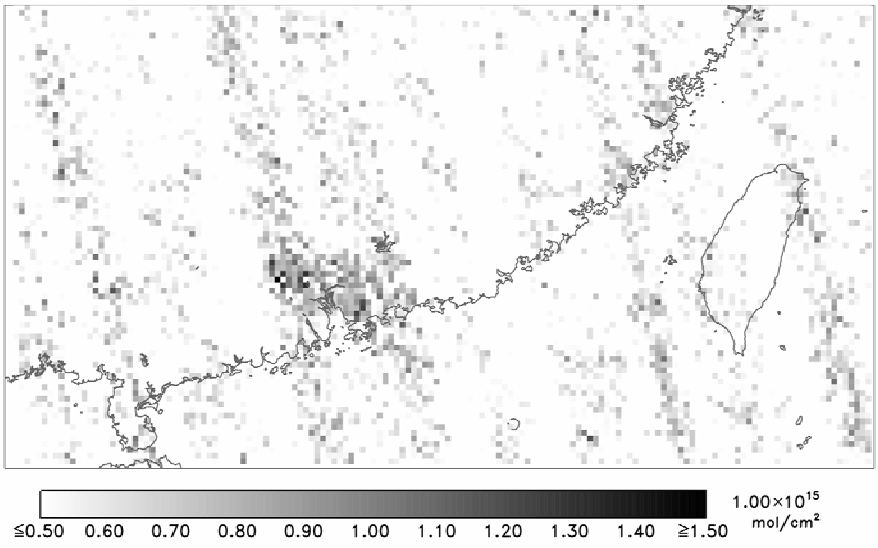

Figure 11. Elevated CHOCHO over the Guangzhou, China area in July, 2005.

7. Requirements for Global Pollution Monitoring

The currently-orbiting satellite instruments which measure the troposphere in the UV/visible from nadir geometry, GOME, SCIAMACHY, and OMI (and design of the OMPS series of instruments), have done much to prepare the way for eventual global and continuous pollution monitoring from space. Robust algorithms for measurement of ozone profiles and tropospheric ozone, NO_2, HCHO, and volcanic SO_2 have been developed, with anthropogenic SO_2 measurement capability under development. Initial measurements of CHOCHO have been made; they should become robust measurement products in the near future. BrO, which has been of primarily stratospheric, and more recently upper tropospheric, interest nonetheless has shown scientifically interesting and readily measurable lower tropospheric features, including BrO from the ice pack and from volcanoes and salt lakes. Global pollution monitoring would almost certainly include infrared measurements as well, particularly of carbon monoxide (CO) and, perhaps, additional ozone measurements.

The following discussion assumes that measurements would be made from geostationary orbit (35,800 km) or, possibly, from inclined 24-hour orbits,

which could make measurements to higher latitudes feasible. At least three instruments would be required for global coverage (six if inclined orbits are used). Spatial resolution requirements will depend upon detailed scientific requirement studies, but they will likely be 10×10 km^2 or smaller. The major tradeoffs are in orbit selection, detector format (linear versus 2-D) and type (CMOS-Si versus CCD), and in scanning mode: even instruments using 2-D detectors would need to raster in order to obtain the required spatial coverage.

The spatial resolution requirement assumed here is: at least 1000 resolution elements in the East-West and North-South directions (i.e., a grid of 1000×1000 elements) for a satellite covering 1/3 of the Earth to latitude limits of $\sim\pm60^{o}$. Any final selection will likely approximate this.

7.1. INSTRUMENT DESIGN

7.1.1. *Scanner*

It is generally desirable to limit the number of mechanisms on a space-based instrument. It is partially for this reason that the OMPS and OMI designs selected the pushbroom technique, employing 2-D detectors (CCDs in both cases), where one CCD dimension is spectral and the other spatial (across-track). The satellite movement then gives the along track variation.[69,70] GOME and SCIAMACHY both employ across-track scanners to achieve spatial coverage. Both scanners are currently working as of this writing: the GOME single-axis scanner for almost 11 years and the SCIAMACHY two-axis scanner for almost 4 years. Thus, the use of a scanning mechanism has been demonstrated to be suitable for use in this application. OMPS will simultaneously measure spectra for 35 across-track ground pixels; OMI measures 60 across-track ground pixels. Neither value is close to what will reasonably be required for geostationary measurement (if they were, a single-axis scanner would still be required). Two-axis scanning will thus be required for successful measurements from geostationary orbit.

7.1.2. *Detectors*

The current generation of satellite spectrometers (summarized above in Table 1) utilizes either 1-dimensional silicon diode array detectors (1024-element Reticon® detectors for GOME and SCIAMACHY) or 2-dimensional CCD devices (OMI and OMPS). Of the two choices, the diode array detectors offer the best performance on a per-pixel basis, having large charge capacities and generally lower dark current. In the most favorable cases, it has been possible to fit GOME spectra, for example, to an RMS of $<3\times10^{-4}$ of the full scale radiance.[14] CCD detectors at present achieve lower performance on a per-pixel

basis but enable multiple spectra to be obtained simultaneously, *i.e.*, spectrum in one dimension and across-track ground pixel position in the other. For low-Earth-orbit measurements they have disadvantages in that the pixel size increases substantial with off-track (*i.e.*, away from nadir) position, and the instrument line shape varies substantially in both the spectral and spatial dimensions. This will be less of a problem for geostationary measurements, assuming that the "across-track" (*i.e*., spatial, or swath) dimension will cover a relatively small fraction of the Earth disk instantaneously, and thus the angular field-of-view of the instrument will be smaller. CCDs are sensitive to degradation from radiation damage. Future instruments employing 2-D detectors may well benefit from the use of 2-D silicon diode array technology which has recently become available in sufficiently large formats, and combines the advantages of both previous types: large 2-D format, high charge capacity (for potentially higher achievable signal-to-noise ratios), and good radiation tolerance. The primary current example is the Rockwell HyViSI® series of CMOS-Si detectors (CMOS-HgCdTe versions are also available for infrared applications). For a recent comparison of CCDs and CMOS detectors see Ref. 71. Linear silicon detectors are now available in larger formats (up to 2048 pixels) with improved performance (*e.g*., Hamamatsu S3904-2048Q). The larger number of pixels allows for extensive wavelength coverage while avoiding spectral undersampling.[26]

7.1.3. *Spectrometer*

The major aspect of spectrometer design that requires improvement applies in the case where 2-D detectors are used. In this case, improved optical design is required to reduce "smile" on the detector arrays, where the spatial and spectral dimensions are not fully orthogonal (and may alias onto one another if the sampling is insufficient), and to reduce the variation of instrument line shape across the spatial dimension.

It would also be useful to consider alternate configurations, for example, where multiple 1-D detectors are used to obtain spectra of different scenes simultaneously. This would improve the characteristics of individual spectra while maintaining at least part of the multiplex advantage of 2-D detectors.

7.2. ORBIT CONSIDERATIONS

A constellation of three satellites in geostationary orbits is commonly considered to be a standard configuration to achieve global coverage up to latitudes limited by viewing angles and physics. Measurements to high latitudes become difficult due to the high viewing zenith angle: The viewing zenith angle for 60^{o} looking directly North or South is already quite high (68^{o}). It increases

to more than 84^o for views 60^o East or West. This makes tropospheric measurements, especially in the UV, quite challenging even under high Sun conditions due to the large contribution of Rayleigh scattering to the measured radiances.

The use of inclined 24-hour orbits could improve this situation, at the cost of more instruments or reduced temporal coverage. For example, a satellite in geostationary orbit at 100^{o}W would effectively cover the U.S. (except for most of Alaska), southern Canada, and South America. Northern Canada would be problematic (as would much of northern Europe for a European member of the constellation). Inclining the orbits to 50^o, with maximum latitude at solar noon, would permit the Northern Hemisphere to be well-covered during most of the day lit parts of the orbits, but would sacrifice coverage of much of the Southern Hemisphere. A second set of satellites with opposite phase would recover this.

8. Conclusions

Issues of instrument requirements (signal-to-noise ratio and spectral resolution) and algorithm physics have largely been addressed in the development of data products for GOME, SCIAMACHY, and OMI. The exact choices for geostationary instruments would need to be made considering the tradeoffs among technical capability, scientific requirements, and cost.

Several algorithm issues remain. These include development of the capability to measure anthropogenic SO_2 and improvements for CHOCHO. The advent (and cost!) of geostationary measurements would also provide an appropriate occasion to revisit some details of fitting algorithms. For example, there remains a degree of arbitrariness among choices of fitting functions for slant column measurements employed for both scientific and operational data products. Choices include directly fitting the radiance R, fitting R/I_0, fitting $ln(R/I_0)$, or fitting a high-pass filtered version of $ln(R/I_0)$ ("DOAS"). All choices are in current use and few data products have benefited from a systematic comparison of choices. A comprehensive review of algorithm physics and reference spectra would also be appropriate to a new program for global measurements.

The major needs for development have been presented in Section 7. The most critical point is that choice of detector type and geometry should proceed together with spectrometer design studies so that the choice is not made prematurely. An alternate orbit choice (inclined 24-hour orbits) has been presented although it may be that it is not seriously considered due to cost.

ACKNOWLEDGEMENTS

The author is grateful to his colleagues for sharing figures to include here: Xiong Liu, Randall V. Martin, Christopher E. Sioris, and Thomas P. Kurosu. He also appreciates ongoing collaborations with colleagues Daniel Jacob, Paul Palmer, Yuhang Wang, Lyatt Jaeglé, Robert Spurr, Michael Newchurch, and many others. Research at the CfA is supported by NASA and the Smithsonian Institution. The cooperation of the European Space Agency and the German Aerospace Center on the GOME and SCIAMACHY programs has been generous, and fundamental to this research. This chapter contains non-copyright material from the author's recent publication "Ultraviolet and visible spectroscopy and spaceborne remote sensing of the Earth's atmosphere," *Comp. Rend. Phys. Special issue on Molecular Spectroscopy and Planetary Atmospheres* 6, 836-847 (2005).

References

1. J.P. Burrows and K.V. Chance, SCanning Imaging Absorption spectroMeter for Atmospheric CHartographY, *Proc. SPIE, Future European and Japanese Remote Sensing Sensors and Programs* 1490, 146-154 (1991).
2. K.V. Chance, J.P. Burrows, and W. Schneider, Retrieval and molecule sensitivity studies for the Global Ozone Monitoring Experiment and the SCanning Imaging Absorption spectroMeter for Atmospheric CHartographY, *Proc. SPIE Remote Sensing of Atmospheric Chemistry* 1491, 151-165 (1991).
3. J. Fishman, A.E. Wozniak, and J.K. Creilson, Global distribution of tropospheric ozone from satellite measurements using the empirically corrected tropospheric ozone residual technique: Identification of the regional aspects of air pollution, *Atmos. Chem. Phys*. 3, 893-907, (2003).
4. J. Fishman, J. K. Creilson, A. E. Wozniak, and P. J. Crutzen, Interannual variability of stratospheric and tropospheric ozone determined from satellite measurements, *J. Geophys. Res*. 110, D20306, doi:10.1029/2005JD005868 (2005).
5. A.J. Krueger, S.J. Schaefer, N. Krotkov, G. Bluth, and S. Barker, Ultraviolet Remote Sensing of Volcanic Emissions, in: *Remote Sensing of Active Volcanism*, edited by P. Mouginis Mark, J.A. Crisp, and J. H. Fink, Geophysical Monograph 116, American Geophysical Union, Washington, DC (2000).
6. M. Eisinger and J.P. Burrows, Tropospheric sulfur dioxide observed by the ERS-2 GOME instrument, *Geophys. Res. Lett*. 25, 4177-4180 (1998).
7. J. Joiner, and P.K. Bhartia, The determination of cloud pressures from rotational Raman scattering in SBUV measurements, *J. Geophys. Res*. 100, 23,019-23,026 (1995).
8. http://www-iup.physik.uni-bremen.de/deu/; http://satellite.iup.uni-heidelberg.de/; http://www.ssd.rl.ac.uk/RSG/; http://www.aeronomie.be/; http://www.knmi.nl/omi/; http://neonet.knmi.nl/neoaf/; http://www.sron.nl/; http://hyperion.gsfc.nasa.gov/; http://www.jcet.umbc.edu/; http://www.caf.dlr.de/caf/institut/dfd/; http://www.esa.int/esaEO/; http://www.space.gc.ca/asc/eng/satellites/
9. R.L. Kurucz, I. Furenlid, J. Brault, and L. Testerman, Solar Flux Atlas from 296 to 1300 nm, National Solar Observatory, Sunspot, New Mexico, 240 pp. (1984).

10. T.N. Woods, D.K. Prinz, G.J. Rottman, J. London, P.C. Crane, R.P. Cebula, E. Hilsenrath, G.E. Brueckner, M.D. Andrews, O.R. White, M.E. VanHoosier, L.E. Floyd, L.C. Herring, B.G. Knapp, C.K. Pankratz, and P.A. Reiser, Validation of the UARS solar ultraviolet irradiances: Comparison with the ATLAS 1 and 2 measurements, *J. Geophys. Res*. 101, 9541-9570 (1996).
11. A. Berk, G.P. Anderson, L.S.Bernstein, P.K. Acharya, H. Dothe, M.W. Matthew, S.M. Adler-Golden, J.H. Chetwynd, Jr., S.C. Richtsmeier, B. Pukall, C.L. Allred, L.S. Jeong, and M.L. Hoke, MODTRAN4 radiative transfer modeling for atmospheric correction, *Proc. SPIE, Optical Spectroscopic Techniques and Instrumentation for Atmospheric and Space Research III* 3756, 348-353 (1999).
12. GOME Users Handbook Manual, ESA Special Publication SP-1182, ESTEC, Noordwijk, The Netherlands (1995).
13. S. Noël, J.P. Burrows, H. Bovensmann, J. Frerick, K.V. Chance, A.P.H. Goede, and C. Muller, Atmospheric trace gas sounding with SCIAMACHY, *Adv. Space Res*. 26, 1949-1954 (2000).
14. K. Chance, Analysis of BrO measurements from the Global Ozone Monitoring Experiment, *Geophys. Res. Lett*. 25, 3335-3338 (1998).
15. U. Platt, Differential Optical Absorption Spectroscopy (DOAS), in: *Air Monitoring by Spectroscopic Techniques*, edited by M.W. Sigrist, Chem. Anal. Ser. 127 (John Wiley, New York, 1994), pp. 27-84.
16. P.I. Palmer, D.J. Jacob, K. Chance, R.V. Martin, R.J.D. Spurr, T.P. Kurosu, I. Bey, R. Yantosca, A. Fiore, and Q. Li, Air mass factor formulation for spectroscopic measurements from satellites: Application to formaldehyde retrievals from the Global Ozone Monitoring Experiment, *J. Geophys. Res*. 106, 14,539-14,550 (2001).
17. R.V. Martin, K. Chance, D.J. Jacob, T.P. Kurosu, R.J.D. Spurr, E. Bucsela, J.F. Gleason, P.I. Palmer, I. Bey, A.M. Fiore, Q. Li, R.M. Yantosca, and R.B.A. Koelemeijer, An improved retrieval of tropospheric nitrogen dioxide from GOME, *J. Geophys. Res*. 107, 4437, doi:10.1029/2001JD0010127 (2002).
18. R. Spurr, M. van Roozendael, J. Lambert, and C. Fayt, The GODFIT direct fitting algorithm: A new approach for total column retrieval, *Proc. 2004 ENVISAT & ERS Symposium*, ESA publication SP-572 (2004).
19. S.F. Singer and R.C. Wentworth, A method for the determination of the vertical ozone distribution from a satellite, *J. Geophys. Res*. 62, 299-308 (1957).
20. D.F. Heath, C.L. Mateer, and A.J. Krueger, The Nimbus-4 backscatter ultraviolet (BUV) atmospheric ozone experiment - two years' operation, *Pure Appl. Geophys*. 106-108, 1238-1253 (1973).
21. K.V. Chance, J.P. Burrows, D. Perner, and W. Schneider, Satellite measurements of atmospheric ozone profiles, including tropospheric ozone, from UV/visible measurements in the nadir geometry: A potential method to retrieve tropospheric ozone, *J. Quant. Spectrosc. Radiat. Transfer* 57, 467-476 (1997).
22. C. Caspar and K. Chance, GOME wavelength calibration using solar and atmospheric spectra, *Proc. Third ERS Symposium on Space at the Service of our Environment*, edited by T.-D. Guyenne and D. Danesy, European Space Agency Special Publication SP-414 (1997).
23. J. Joiner, P.K. Bhartia, R.P. Cebula, E. Hilsenrath, R.D. McPeters, and H. Park, Rotational Raman scattering (Ring effect) in satellite backscatter ultraviolet measurements, *Appl. Opt*. 34, 4513-4525 (1995).
24. K. Chance and R.J.D. Spurr, Ring effect studies: Rayleigh scattering, including molecular parameters for rotational Raman scattering, and the Fraunhofer spectrum, *Appl. Opt*. 36, 5224-5230 (1997).

25. M. Vountas, V.V. Rozanov, and J.P. Burrows, Ring effect: Impact of rotational Raman scattering on radiative transfer in Earth's Atmosphere, *J. Quant. Spectrosc. Radiat. Transfer* 60, 943-961 (1998).
26. K. Chance, T.P. Kurosu, and C.E. Sioris, Undersampling correction for array detector-based satellite spectrometers, *Appl. Opt.* 44, 1296-1304 (2005).
27. L.A. Hall, and G.P. Anderson, High-resolution solar spectrum between 200 and 3100 Å, *J. Geophys. Res*. 96, 12,927-12,931 (1991).
28. D.R. Bates, Rayleigh scattering by air, *Planet. Space Sci*. 32, 785-790 (1984).
29. B.A. Bodhaine, N.B. Wood, E.G. Dutton, and J.R. Slusser, On Rayleigh optical depth calculations, *J. Atmos. Ocean. Tech*. 16, 1854-1861 (1999).
30. J.F. Grainger and J. Ring, Anomalous Fraunhofer line profiles, *Nature* 193, 762 (1962).
31. A.P. Vasilkov, J. Joiner, J. Gleason, and P.K. Bhartia, Ocean Raman scattering in satellite backscatter UV measurements, *Geophys. Res. Lett*. 29, 1837, doi:10.1029/2002GL014955 (2002).
32. L.S. Rothman, D. Jacquemart, A. Barbe, D. Chris Benner, M. Birk, L.R. Brown, M.R. Carleer, C. Chackerian, Jr., K. Chance, L.H. Coudert, V. Dana, V.M. Devi, J.-M. Flaud, R.R. Gamache, A. Goldman, J.-M. Hartmann, K.W. Jucks, A.G. Maki, J.-Y. Mandin, S.T. Massie, J. Orphal, A. Perrin, C.P. Rinsland, M.A.H. Smith, J. Tennyson, R.N. Tolchenov, R.A. Toth, J. Vander Auwera, P. Varanasi, and G. Wagner, The HITRAN 2004 molecular spectroscopic database, *J. Quant. Spectrosc. Radiat. Transfer* 96, 139-204 (2005).
33. J. Orphal and K. Chance, Ultraviolet and visible absorption cross sections for HITRAN, *J. Quant. Spectrosc. Radiat. Transfer* 82, 491-504 (2003).
34. S. Goldman, *Information Theory* (Prentice-Hall, New York, 1953).
35. S. Slijkhuis, A. von Bargen, W. Thomas, and K. Chance, Calculation of undersampling correction spectra for DOAS spectral fitting, *Proc. ESAMS'99 - European Symposium on Atmospheric Measurements from Space*, 563-569 (1999).
36. R.J.D. Spurr, T.P. Kurosu, and K. Chance, A linearized discrete ordinate radiative transfer model for atmospheric remote sensing retrieval, *J. Quant. Spectrosc. Radiat. Transfer* 68, 689-735 (2001).
37. R.J.D. Spurr, LIDORT V2PLUS: A comprehensive radiative transfer package for UV/VIS/NIR nadir remote sensing; A general quasi analytic solution, *Proc. SPIE, Remote Sensing of Clouds and the Atmosphere VIII* 5235 (2003).
38. R.F. Van Oss and R.J.D. Spurr, Fast and accurate 4-stream linearized discrete ordinate radiative transfer models for ozone profile retrieval, *J. Quant. Spectrosc. Radiat. Transfer* 75, 177-220 (2002).
39. V.V. Rozanov, D. Diebel, R.J.D. Spurr, and J.P. Burrows, GOMETRAN: A radiative transfer model for the satellite project GOME - the plane-parallel version, *J. Geophys. Res*. 102, 16,683-16,695 (1997).
40. V.V. Rozanov, M. Buchwitz, K.-U. Eichmann, R. de Beek, and J.P. Burrows, SCIATRAN - a new radiative transfer model for geophysical applications in the 240-2400 nm spectral region: The pseudo-spherical version, *Adv. Space Res*. 29, 1831-1835 (2002).
41. C.A. McLinden, J.C. McConnell, E. Griffioen, and C.T. McElroy, A vector radiative transfer model for the Odin/OSIRIS project, *Can. J. Phys*. 80, 375-393 (2002).
42. J.F. De Haan, P.B. Bosma, and J.W. Hovenier, The adding method for multiple scattering calculations of polarized light, *Astron. Astrophys*. 183, 371-391 (1987).
43. P. Stammes, Spectral radiance modelling in the UV-visible range, in: *IRS 2000: Current Problems in Atmospheric Radiation*, edited by W.L. Smith and Y.M. Timofeyev (A. Deepak, Hampton, VA, 2001), pp. 385-388.

44. I. Bey, D.J. Jacob, R.M. Yantosca, J.A. Logan, B.D. Field, A.M. Fiore, Q. Li, H.Y. Liu, L.J. Mickley, and M.G. Schultz, Global modeling of tropospheric chemistry with assimilated meteorology: Model description and evaluation, *J. Geophys. Res*. 106, 23,073-23,096 (2001).
45. G.P. Brasseur, D.A. Hauglustaine, S. Walters, P.J. Rasch, J.-F. Muller, C. Granier, and X.X. Tie, MOZART: A global chemical transport model for ozone and related chemical tracers, Part 1. Model description, *J. Geophys. Res. 103*, 28,265-28,289 (1998).
46. D.A. Hauglustaine, G.P. Brasseur, S. Walters, P.J. Rasch, J.-F. Muller, L.K. Emmons, and M.A. Carroll, MOZART: A global chemical transport model for ozone and related chemical tracers, Part 2. Model results and evaluation, *J. Geophys. Res*. 103, 28,291-28,335 (1998).
47. A.J. Fleig, R.D. McPeters, P.K. Bhartia, B.M. Schlesinger, R.P. Cebula, K.F. Klenk, S.L. Taylor, and D.F. Heath, Nimbus-7 Solar Backscatter Ultraviolet (SBUV) Ozone Products User's Guide, NASA Reference Publication, 1234, National Aeronautics and Space Administration, Washington, DC (1990).
48. R.D. McPeters, A.J. Krueger, P.K. Bhartia, and J.R. Herman, Earth Probe Total Ozone Mapping Spectrometer (TOMS) Data Products User's Guide, NASA Reference Publication 1998-206895, National Aeronautics and Space Administration, Washington, DC (1998).
49. R. Munro, R. Siddans, W.J. Reburn, and B. Kerridge, Direct measurement of tropospheric ozone from space, *Nature* 392, 168-191 (1998).
50. X. Liu, K. Chance, C.E. Sioris, R.J.D. Spurr, T.P. Kurosu, R.V. Martin, and M.J. Newchurch, Ozone profile and tropospheric ozone retrievals from Global Ozone Monitoring Experiment: Algorithm description and validation, *J. Geophys. Res*. 110, D20307, doi:10.1029/2005JD006240 (2005).
51. X. Liu, K. Chance, C.E. Sioris, T.P. Kurosu, R.J.D. Spurr, R.V. Martin, M. Fu, J.A. Logan, D.J. Jacob, P.I. Palmer, M.J. Newchurch, I. Megretskaia, and R. Chatfield, First directly-retrieved global distribution of tropospheric column ozone from GOME: Comparison with the GEOS-CHEM model, *J. Geophys. Res*., in press (2006).
52. W. Thomas, E. Hegels, S. Slijkhuis, R. Spurr, and K. Chance, Detection of biomass burning combustion products in Southeast Asia from backscatter data taken by the GOME spectrometer, *Geophys. Res. Lett*. 25, 1317-1320 (1998).
53. C.E. Sioris, T.P. Kurosu, R.V. Martin and K. Chance, Stratospheric and tropospheric NO_2 observed by SCIAMACHY: First results, *Adv. Space Res. Special issue: Trace Constituents in the Troposphere and Lower Stratosphere* 34/4, 780-785 (2004).
54. R.V. Martin, D.J. Jacob, K. Chance, T.P. Kurosu, P.I. Palmer, and M.J. Evans, Global inventory of nitrogen oxide emissions constrained by space-based observations of NO_2 columns, *J. Geophys. Res*. 108(D17), 4537, doi:10.1029/2003JD003453 (2003).
55. R.V. Martin, D.D. Parrish, T.B. Ryerson, D.K. Nicks Jr., K. Chance, T.P. Kurosu, A. Fried, B.P. Wert, D.J. Jacob, and E.D. Sturges, Evaluation of GOME satellite measurements of tropospheric NO_2 and HCHO using regional data from aircraft campaigns in the southeastern United States, *J. Geophys. Res*. 109, D24307, doi:10.1029/2004JD004869 (2004).
56. L. Jaeglé, L. Steinberger, R.V. Martin, and K. Chance, Global partitioning of NO_x sources using satellite observations: Relative roles of fossil fuel combustion, biomass burning and soil emissions, *Faraday Discuss*. 130, 407-423, doi:10.1039/b502128f (2005).
57. L. Jaeglé, R.V. Martin, K. Chance, L. Steinberger, Kurosu, T.P., D.J. Jacob, A.I. Modi, V. Yoboué, L. Sigha-Nkamdjou, and C. Galy-Lacaux, Satellite mapping of rain-induced nitric oxide emissions from soils, *J. Geophys. Res*. 109, D21310, doi:10.1029/2004JD004787 (2004).
58. Y. Choi, Y. Wang, T. Zeng, R.V. Martin, T.P. Kurosu, and K. Chance, Evidence of lightning NO_x and convective transport of pollutants in satellite observations over North America, *Geophys. Res. Lett*. 32, L02805, doi:10.1029/2004GL021436 (2005).

59. K. Kreher, P.V. Johnston, S.W. Wood, B. Nardi, and U. Platt, Ground-based measurements of tropospheric and stratospheric BrO at Arrival Heights, Antarctica, *Geophys. Res. Lett*. 24, 3021-3024, 1997.
60. T. Zeng, Y. Wang, K. Chance, E.V. Browell, B.A. Ridley, and E.L. Atlas, Widespread persistent near-surface O_3 depletion at northern high latitudes in spring, *Geophys. Res. Lett*. 30(24), 2298, doi:10.1029/2003GL018587 (2003).
61. V. Matveev, M. Peleg, D. Rosen, D.S. Tov-Alper, K. Hebestreit, J. Stutz, U. Platt, D. Blake, and M. Luria, Bromine oxide - ozone interaction over the Dead Sea, *J. Geophys. Res.* 106, 10,375-10,387 (2001).
62. J. Stutz, R. Ackermann, J.D. Fast, and L.A. Barrie, Atmospheric reactive chlorine and bromine at the Great Salt Lake, Utah, *Geophys. Res. Lett.* 29(10), doi:10.1029/2002GL014812 (2002).
63. N. Bobrowski, G. Hönninger, B. Galle, and U. Platt, Detection of bromine monoxide in a volcanic plume, *Nature* 423, 273-276 (2003).
64. K. Chance, P. Palmer, R.J.D. Spurr, R.V. Martin, T. Kurosu, and D.J. Jacob. Satellite observations of formaldehyde over North America from GOME, *Geophys. Res. Lett*. 27, 3461-3464 (2000).
65. P.I. Palmer, D.J. Jacob, A.M. Fiore, R.V. Martin, K. Chance, and T. Kurosu, Mapping isoprene emissions over North America using formaldehyde column observations from space, *J. Geophys. Res*. 108, 4180, doi:10.1029/2002JD002153 (2003).
66. D.S. Abbot, P.I. Palmer, R.V. Martin, K.V. Chance, D.J. Jacob, and A. Guenther, Seasonal and interannual variability of isoprene emissions as determined by formaldehyde column measurements from space, *Geophys. Res. Lett*. 30, 1886, doi:10.1029/2003GL017336 (2003).
67. C. Shim, Y. Wang, Y. Choi, P.I. Palmer, D.S. Abbot, and K. Chance, Constraining global isoprene emissions with GOME HCHO column measurements, *J. Geophys. Res*. 110, D24301, doi:10.1029/2004JD005629 (2005).
68. R. Volkamer, L.T. Molina, M.J. Molina, T. Shirley, and W.H. Brune, DOAS measurement of glyoxal as an indicator for fast VOC chemistry in urban air, *Geophys. Res. Lett*. 32, L08806, doi:10.1029/2005GL022616 (2005).
69. M.G. Dittman, E. Ramberg, M. Chrisp, J.V. Rodriguez, A.L. Sparks, N.H. Zaun, P. Hendershot, T. Dixon, R.H. Philbrick, and D. Wasinger, Nadir ultraviolet imaging spectrometer for the NPOESS Ozone Mapping and Profiler Suite (OMPS), *Proc. SPIE Earth Observing Systems VII* 4814, 111-119 (2002).
70. P.F. Levelt, G.H.J. van den Oord, M.R. Dobber, A. Malkki, H. Visser, J. de Vries, P. Stammes, J. Lundell, and H. Saari, The Ozone Monitoring Instrument, *IEEE Transactions on Geoscience and Remote Sensing*, in press (2006).
71. P. Magnan, Detection of visible photons in CCD and CMOS: A comparative view, *Nucl. Instrum. Meth. Phys. Res. A* 504, 199-212 (2003).